Yerevan State University

Department of Physics

Investigating Quantum Hardware Using Microwave Pulses

Student:
Diana Avetisyan

Supervisor:
Hakob Avetisyan

Head of Chair:
Aram Saharian

Abstract

In this Diploma I describe the physics of the two level systems and use them to demonstrate some experiments on the IBM quantum hardware. Namely, I find and measure qubit frequency, calibrate pulses to form quantum gates, measure qubit lifetime T_1 and decoherence time T_2, and eliminate quasi-static noise by a technique called dynamical decoupling. After reviewing the necessary theory for the two-level systems I perform a Rabi as well as Ramsey experiments, and mitigate the errors using dynamical decoupling. Afterwards I perform experiments on one of the quantum computers of IBM, including finding the qubit frequency using frequency sweep algorithm, then finding the best amplitude by doing the Rabi π-pulse experiment. After finding the perfect measure the T_1 and T_2, via Ramsey experiment and eventually mitigate the errors using dynamical decoupling. By comparing the theory with the experiment, we conclude that the theory for the two-level systems perfectly works for the qubits.

Signature Page

Student: _____

Diana Avetisyan

Supervisor: _____

Hakob Avetisyan

Allow to Protection

Head of the Chair: _____

Aram Saharian

Contents

1 Theoretical Part: Introduction

Computers are getting smaller and faster day by day because electronic components are getting smaller and smaller. But this process is about to meet its physical limit, and since the size of transistors is shrinking to size of few atoms, transistors cannot be used as switch because electrons may transfer themselves to the other side of blocked passage by the process called quantum tunnelling.
Quantum mechanics is a branch of physics that explores physical world at most fundamental level. At this level particles behave differently from classical world: they can be in a superposition of more than one states, and interact with other particles, that are very far away, so strongly that classical physics cannot explain. These phenomena are called superposition and entanglement. More than two decades ago researchers entertained the idea whether one can use these new features to do something useful [1]. Since then, the field of quantum technologies has emerged and now engineers are building various devises for computation, communication, sensing and simulation using quantum systems [2].
What can quantum computers do?

1. They can easily crack the encryption algorithms used today efficiently whereas it takes billions of years to best supercomputer available today. Even though quantum computers would be able to crack many of today's encryption techniques, predictions are that they would create hack-proof replacements [3].

2. They are great for solving optimization problems, although the speedups expected from quantum computers are moderate [4].

3. They can simulate other quantum or classical systems efficiently, a task of major importance in, e.g., biology and chemistry [5].

There is a great advancement in building, sometimes even providing access to quantum computers. Examples of quantum computers made of different physical system can be found in [6].

One can even access and manipulate quantum computers. For example, IBM Quantum offers a public cloud access to their quantum computers consisting of up to 16 qubits [7]. The quantum computers one interacts with in IBM Quantum use a physical type of qubit called a superconducting transmon qubit, which is made from superconducting materials such as niobium and aluminum, patterned on a silicon substrate. Superconducting qubits are electrical circuits that behave like atoms. Essentially superconducting qubits are non-linear oscillators built from inductors and capacitors. The inductor is realized by a Josephson junction, a nonlinear inductor that makes the resonator anharmonic. Anharmonic oscillators feature in addressable two level system. The qubit states can either be states of phase across the Josephson Junction, flux in a superconducting loop, or even charge on the Junction island. The qubit formed by isolating two energy levels out of many levels of the anharmonic oscillator.

The difference in energy between these two energy levels sets the characteristic frequency ν of the qubit through Planck's constant h: $\Delta E = h\nu$. These frequencies are nominally targeted to be around $5GHz$. For a superconducting qubit to behave as the abstract notion of the qubit, one must have the device at drastically low temperatures T such that $k_B T \ll h\nu$, where k_B is Boltzmann's constant. In the IBM Quantum lab, they must keep the temperature extremely cold (15 millikelvin in a dilution refrigerator) to minimize ambient noise or heat that could excite the superconducting qubit and increase the error probability. Once a system has cooled to the target temperature, which takes several days, the qubit reaches equilibrium at the ground state $|0\rangle$.

In this Diploma, I will briefly describe the physics of the two level systems and use them to demonstrate some experiments on the IBM quantum hardware. Namely, to find and measure the qubit frequency, to calibrate pulses to form quantum gates, to measure qubit lifetime T_1 and decoherence time T_2, and to eliminate quasi-static noise by a technique called dynamical decoupling.

2 Qubits and Pulses to Control Them

2.1 The Rabi Model

Before approaching Rabi's model we will start with discussion of general study of two-level system. Examples of two-level quantum systems are [6]

- Spin 1/2 particles,
- "Two level" atoms which is an atom driven with an oscillating electromagnetic field whose frequency closely matches one of the atomic transition frequencies,
- A particle in a double wall potential.

Consider a qubit, a system with two quantum energy levels. The Hamiltonian H_0 of the qubit has eigenstates that satisfy

$$H_0|0\rangle = \hbar\omega_0|0\rangle, \tag{1}$$

$$H_0|1\rangle = \hbar\omega_1|1\rangle, \tag{2}$$

so that

$$H_0 = \hbar\omega_0|0\rangle\langle 0| + \hbar\omega_1|1\rangle\langle 1|. \tag{3}$$

In the $\{|0\rangle, |1\rangle\}$ basis, H_0 is represented by the matrix:

$$H_0 = \hbar \begin{pmatrix} \omega_0 & 0 \\ 0 & \omega_1 \end{pmatrix}. \tag{4}$$

The evolution of the qubit, initially in a state $|\psi(0)\rangle$, is governed by the unitary operator $U(t, t_0) = e^{-iH_0 t/\hbar}$:

$$\begin{aligned} |\psi(t)\rangle &= e^{-iH_0 t/\hbar}|\psi(0)\rangle \\ &= e^{-iH_0 t/\hbar}(|0\rangle\langle 0| + |1\rangle\langle 1|)|\psi(0)\rangle \\ &= e^{-i\omega_0 t}|0\rangle\langle 0|\psi(0)\rangle + e^{-i\omega_1 t}|1\rangle\langle 1|\psi(0)\rangle \\ &\equiv c_0 e^{-i\omega_0 t}|0\rangle + c_1 e^{-i\omega_1 t}|1\rangle, \end{aligned} \tag{5}$$

where in the second line we used the resolution of identity $I = |0\rangle\langle 0| + |1\rangle\langle 1|$, and in the last line we defined $c_0 = \langle 0|\psi(0)\rangle$ and $c_1 = \langle 1|\psi(0)\rangle$.

Let's now add a time independent external field W on the Hamiltonian. W is represented by a Hermitian matrix:

$$W = \begin{pmatrix} W_{00} & W_{01} \\ W_{10} & W_{11} \end{pmatrix}, \tag{6}$$

where W_{00} and W_{11} are real, moreover

$$W_{01} = W_{10}^*. \tag{7}$$

As a result we get:

$$W = \begin{pmatrix} W_{00} & W_{01} \\ W_{01}^* & W_{11} \end{pmatrix}, \tag{8}$$

$$H = H_0 + W = \begin{pmatrix} \hbar\omega_0 + W_{00} & W_{01} \\ W_{01}^* & \hbar\omega_1 + W_{11} \end{pmatrix}. \tag{9}$$

Adding a constant to energy is equivalent to choosing a zero state energy. Let's choose

$$E_{gnd} = -\frac{1}{2}(\hbar\omega_0 + W_{00} + \hbar\omega_1 + W_{11}) \tag{10}$$

as a ground state energy. Which gives

$$H = \begin{pmatrix} \frac{1}{2}(\hbar\omega_0 + W_{00} - \hbar\omega_1 - W_{11}) & W_{01} \\ W_{10} & -\frac{1}{2}(\hbar\omega_0 + W_{00} - \hbar\omega_1 - W_{11}) \end{pmatrix} \tag{11}$$

Let's introduce new variables

$$\Delta = \Big(\omega_1 + \frac{W_{11}}{\hbar} - \omega_0 - \frac{W_{00}}{\hbar}\Big), \qquad \Omega = \frac{2W_{10}}{\hbar}, \tag{12}$$

where Δ is called detuning, the energy spacing between the perturbed levels $|\omega_0\rangle$ and $|\omega_1\rangle$ and Ω is the strength of coupling between them, the so called Rabi frequency. The Hamiltonian then will be

$$H = \frac{\hbar}{2}\begin{pmatrix} -\Delta & \Omega \\ \Omega^* & \Delta \end{pmatrix}. \tag{13}$$

A system described by this Hamiltonian is the most general model of a time independent two-level system, and it is called the Rabi model.

2.1.1 Finding the Eigenvalues and Eigenstates of the System

Let's now find the eigenvalues of the system using the following equation or diagonalization of equation:

$$\begin{pmatrix} -\Delta/2 - \omega_\pm & \Omega^*/2 \\ \Omega/2 & \Delta/2 - \omega_\pm \end{pmatrix}\begin{pmatrix} |\psi_+\rangle \\ |\psi_-\rangle \end{pmatrix} = 0, \tag{14}$$

$$\det\begin{vmatrix} -\Delta/2 - \omega_\pm & \Omega^*/2 \\ \Omega/2 & \Delta/2 - \omega_\pm \end{vmatrix} = 0, \tag{15}$$

$$(-\Delta/2 - \omega_\pm)(\Delta/2 - \omega_\pm) - \frac{|\Omega|^2}{4} = 0, \tag{16}$$

$$\omega_\pm = \pm\frac{1}{2}\sqrt{\Delta^2 + |\Omega|^2}. \tag{17}$$

Now after inserting the expressions for Δ and Ω and adding the ground state energy recall that

$$\begin{aligned} E_+ = &\frac{1}{2}(E_0 + W_{00} + E_1 + W_{11}) \\ &+ \frac{1}{2}\sqrt{(E_0 + W_{00} - E_1 - W_{11})^2 + 4|W_{01}|^2}, \end{aligned} \tag{18}$$

$$\begin{aligned} E_- = &\frac{1}{2}(E_0 + W_{00} + E_1 + W_{11}) \\ &- \frac{1}{2}\sqrt{(E_0 + W_{00} - E_1 - W_{11})^2 + 4|W_{01}|^2}. \end{aligned} \tag{19}$$

Notice that if $W = 0$, E_+ and E_- are identical to E_0 and E_1. The corresponding eigenstates are found by solving (14) using (17)

$$|\psi_+\rangle = \cos\frac{\theta}{2}e^{-\frac{i\phi}{2}}|0\rangle + \sin\frac{\theta}{2}e^{-\frac{i\phi}{2}}|1\rangle, \tag{20}$$

$$|\psi_-\rangle = -\sin\frac{\theta}{2}e^{-\frac{i\phi}{2}}|0\rangle + \cos\frac{\theta}{2}e^{-\frac{i\phi}{2}}|1\rangle. \tag{21}$$

These states represent antipodal points on a Bloch sphere. The angles θ and ϕ are defined by

$$\tan\theta = \frac{2|W_{01}|}{E_0 + W_{00} - E_1 - W_{11}}, \tag{22}$$

$$W_{10} = |W_{10}|e^{i\phi}, \tag{23}$$

which means that one can position/manipulate the qubit on the Bloch sphere by appropriately choosing the matrix elements of the external field W.

2.1.2 Graphical Representation of the Effect of Coupling

Now, to simplify the discussion let's assume that $W_{00} = W_{11} = 0$ which means that there is no coupling between $|0\rangle$ and $|1\rangle$ states. The formulas (18) and (19) will then be

$$E_+ = \frac{1}{2}\sqrt{(E_0 - E_1)^2 + |W_{01}|^2} \tag{24}$$

$$E_- = -\frac{1}{2}\sqrt{(E_0 - E_1)^2 + |W_{01}|^2} \tag{25}$$

$$\tan\theta = \frac{2|W_{01}|}{E_0 - E_1} \tag{26}$$

We now intend to study the effect of coupling W on the energies E_+ and E_- in terms of the values of E_0 and E_1. Assume that W_{01} is fixed and introduce the two parameters:

$$\begin{aligned} E_m &= \frac{1}{2}(E_0 + E_1) \\ \delta &= \frac{1}{2}(E_0 - E_1) \end{aligned} \tag{27}$$

We see immediately form (2.1.2) and (2.1.2) that the variation of E_+ and E_- with respect to E_m is extremely simple: changing E_m reduces to shifting

the origin along the energy axis. Moreover, it can be verified from (2.1.3), (2.1.3), (22) and (101) that the vectors $|\psi_+\rangle$ and $|\psi_-\rangle$ do not depend on E_m. We are therefore concerned with the influence of the parameter δ, the four energies E_0, E_1, E_+, E_-. We thus obtain for E_0 and E_1 two straight lines of slope $+1$ and -1 (shown in dash in figure 1). Substituting into and we find:

$$E_+ = E_m + \sqrt{\delta^2 + |W_{01}|^2} \tag{28}$$

$$E_- = E_m + \sqrt{\delta^2 + |W_{01}|^2} \tag{29}$$

When δ varies, E_+ and E_- describe the two branches of a hyperbola which is symmetrical with respect to coordinate axis and whose asymptotes are the two straight lines associated with the unperbuted levels; the minimum separation between the two branches is $2|W_{01}|$ (solid lines in figure 1).

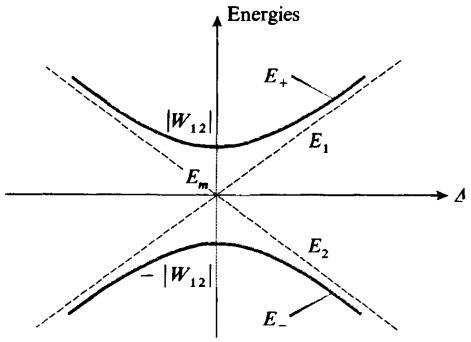

Figure 1: Variation of the energies E_+ and E_- with respect to the energy difference $\Delta = (E_0 - E_1)/2$. In the absence of coupling, the levels cross at the origin (dashed straight lines). Under the effect of the non-diagonal coupling W, the two perturbed levels "repel each other" and we obtain an "anti-crossing": the curves giving E_+ and E_- in terms of Δ are branches of a hyperbola (solid lines in the figure) whose asymptotes are the unperturbed levels.

In the absence of coupling, the energies E_0 and E_1 of the two levels "cross" at $\delta = 0$. It is clear from figure 1 that under the effect of coupling, the two levels "repel each other" - that is, the energy values move further away from each other. The diagram in solid lines in figure 1 is often called an anti-crossing diagram. Also we see that, for any δ we have: $|E_+ - E_-| \geq$

$|E_0 - E_1|$ This is a result which appears rather often in other domains of physics (for example, in electrical circuit theory): the coupling separates the normal frequencies. Near the asymptotes, that is, for $|\delta| \gg |W_{01}|$, formulas and can be written in the form of a limited power series expansion in $\left|\frac{W_{01}}{\delta}\right|$:

$$E_+ = E_m + \delta\Big(1 + \frac{1}{2}\left|\frac{W_{01}}{\delta}\right| + ...\Big) \tag{30}$$

$$E_- = E_m - \delta\Big(1 + \frac{1}{2}\left|\frac{W_{01}}{\delta}\right| + ...\Big) \tag{31}$$

On the other hand, at the center of the hyperbola, for $E_2 = E_1$ $(\delta = 0)$, formulas and yield:

$$E_+ = E_m + |W_{01}| E_- = E_m - |W_{01}| \tag{32}$$

Therefore, the effect of coupling is much more important when the two unperbuted levels have the same energy. The effect is then of the first order, as can be seen from , while it is of second order when $\delta \gg |W_{01}|$ [formulas]. When is used, formula becomes:

$$\tan\theta = \frac{|W_{01}|}{\delta} \tag{33}$$

It follows that, when $\delta \ll |W_{01}|$ (strong coupling), $\theta \simeq \pi/2$. The qubit is on the equator of the Bloch sphere. At the center of the hyperbola, when $E_1 = E_0$ $(\delta = 0)$, we have:

$$|\psi_+\rangle = \frac{1}{\sqrt{2}}\Big[e^{-i\phi/2}|0\rangle + e^{i\phi/2}|1\rangle\Big] \tag{34}$$

$$|\psi_-\rangle = \frac{1}{\sqrt{2}}\Big[-e^{-i\phi/2}|0\rangle + e^{i\phi/2}|1\rangle\Big] \tag{35}$$

On the other hand, when $\delta \gg |W_{01}|$ (weak coupling), $\theta \simeq 0$ (assuming $\delta \geq 0$).

Near the asymptotes (that is, for $\delta \gg |W_{01}|$), we have, to first order in $\frac{|W_{01}|}{\delta}$:

$$|\psi_+\rangle = e^{-i\phi/2}\Big[|0\rangle + e^{i\phi}\frac{|W_{01}|}{2\delta}|1\rangle + ...\Big] \tag{36}$$

$$|\psi_-\rangle = e^{i\phi/2}\Big[|1\rangle + e^{-i\phi}\frac{|W_{01}|}{2\delta}|0\rangle + ...\Big] \tag{37}$$

In other words, for a weak coupling ($E_0 - E_1 \gg |W_{01}|$), the perturbed states differ very slightly from the unperturbed states. We see from (39) and (40) that to within a global phase factor $e^{-i\phi/2}$, $|\psi_+\rangle$ is equal to the state $|0\rangle$ slightly "contaminated" by a small contribution from the state $|1\rangle$. On the other hand, for a strong coupling, formulas indicate that the states $|\psi_+\rangle$ and $|\psi_-\rangle$ are very different from the states $|0\rangle$ and $|1\rangle$, since they are linear superpositions of them with coefficients of the same modulus. Thus, like the energies, the eigenstates undergo significant modifications in the neighborhood of the point where the two unperturbed states cross.

2.1.3 Dynamical Aspect: Oscillation of the System Between the Two Unperturbed States

Let

$$|\psi(t)\rangle = a_0(t)|0\rangle + a_1(t)|1\rangle \tag{38}$$

be the state vector of the system at the instant t. The evolution of $|\psi(t)\rangle$ in the presence of the coupling W is given by the Schrodinger equation:

$$i\hbar\frac{d}{dt}|\psi(t)\rangle = (H_0 + W)|\psi(t)\rangle \tag{39}$$

Let us project this equation onto the basis vectors $|0\rangle$ and $|1\rangle$. We obtain, using (setting $W_{00} = W_{11} = 0$) and

$$i\hbar\frac{d}{dt}a_0(t) = E_0 a_0(t) + W_{01}a_1(t) \tag{40}$$

$$i\hbar\frac{d}{dt}a_1(t) = W_{01}a_0(t) + E_1 a_1(t). \tag{41}$$

If $|W_{01}| \neq 0$, these equations constitute a linear system of homogeneous coupled differential equations. The classical method of solving such a system reduces, to looking for the eigenvectors $|\psi_+\rangle$ and $|\psi_-\rangle$ of the operator $H = H_0 + W$ (whose matrix elements are the coefficients of equations), and decompose $|\psi(0)\rangle$ in terms of $|\psi_+\rangle$ and $|\psi_-\rangle$:

$$|\psi(0)\rangle = \lambda|\psi_+\rangle + \mu|\psi_-\rangle \tag{42}$$

where λ and μ are fixed by the initial coefficients. We then have:

$$|\psi(t)\rangle = \lambda e^{-iE_+t/\hbar}|\psi_+\rangle + \mu e^{-iE_-t/\hbar}|\psi_-\rangle \tag{43}$$

which enables us to obtain $a_1(t)$ and $a_2(t)$ by projecting $|\psi(t)\rangle$ onto $|0\rangle$ and $|1\rangle$. It can be shown that a system whose state vector is the vector $|\psi(t)\rangle$ given in (46) oscillates between the two unperturbed states $|0\rangle$ and $|1\rangle$. To see this, we shall assume that the system at tome $t = 0$ is in the state $|0\rangle$:

$$|\psi(0)\rangle = |0\rangle \tag{44}$$

and calculate the probability $p_{01}(t)$ of finding it in the state $|1\rangle$ at time t. Now let's to find the $p_{01}(t)$, the probability of finding $|\psi\rangle$ in excited state at time t. To do that let us expand the state $|\psi(0)\rangle$ given in on the $\{|\psi_+\rangle; |\psi_-\rangle\}$ basis. Inverting formulas and , we obtain:

$$|\psi(0)\rangle = e^{i\phi/2}\Big[\cos\Big(\frac{\theta}{2}\Big)|\psi_+\rangle + \sin\Big(\frac{\theta}{2}\Big)|\psi_-\rangle\Big] \tag{45}$$

Then deduce, using :

$$|\psi(t)\rangle = e^{i\phi/2}\Big[\cos\Big(\frac{\theta}{2}\Big)e^{-iE_+t/\hbar}|\psi_+\rangle - \sin\Big(\frac{\theta}{2}\Big)e^{-iE_-t/\hbar}|\psi_-\rangle\Big] \tag{46}$$

The probability amplitude of finding the system at time t in the state $|1\rangle$ is then written:

$$\begin{aligned}\langle 1|\psi(t)\rangle &= e^{i\phi/2}\Big[\cos\Big(\frac{\theta}{2}\Big)e^{-iE_+t/\hbar}\langle 1|\psi_+\rangle - \sin\Big(\frac{\theta}{2}\Big)e^{-iE_-t/\hbar}\langle 1|\psi_-\rangle\Big] \\ &= e^{i\phi}\sin\Big(\frac{\theta}{2}\Big)\cos\Big(\frac{\theta}{2}\Big)[e^{-iE_+t/\hbar} - e^{-iE_-t/\hbar}] \end{aligned} \tag{47}$$

which enables us to calculate $p_{01}(t) = |\langle 1|\psi(t)\rangle|^2$. We thus find:

$$p_{01}(t) = \frac{1}{2}\sin^2\theta\Big[1 - \cos\Big(\frac{E_+ - E_-}{\hbar}t\Big)\Big] \tag{48}$$

or, using the expressions

$$p_{01}(t) = \frac{4|\Omega|^2}{4|\Omega| + \delta^2}\sin^2\Big[\frac{t}{2\hbar}\sqrt{4|\Omega|^2 + \delta^2}\Big] \tag{49}$$

Equation is sometimes called Rabi's formula [8].

2.2 Ramsey Experiment

We will now consider in detail the simplest field pulse configuration, invented by N. Ramsey [9]. This configuration consists of the application of a sequence of two pulses to the qubit, that is, a field of the form $E\cos(\omega_0 t)$ which is applied into two pulses: a first $\pi/2$ pulse between $t = 0$ and t_1, then a second $\pi/2$ pulse between T and $T + t_1$. The qubit evolves freely during the time interval $T - t_1$ between the pulses, which is long compared to the pulse length t_1. We will study the evolution of the Bloch vector in the reference frame which rotates at the frequency of the applied field, supposing that the atom is initially in state $|0\rangle$ (see figure 2).

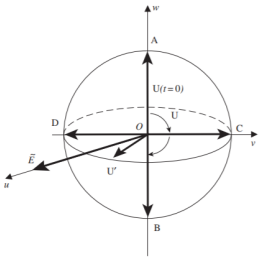

Figure 2: Evolution of the Bloch vector for an atom subjected to two $\pi/2$ pulses separated by a free-evolution time T in the reference frame rotating at a frequency ω of the applied field. At the end of the first pulse, the head of the Bloch vector lies close to point C. In the resonant case the Bloch vector remains fixed between the two pulses, whereas in the non-resonant case it rotates in the plane uOv until position U'.

Let us first treat the case of exact resonance: $\omega = \omega_0$. The first $\pi/2$ pulse causes the head of the Bloch vector to pass from point A to point C on the v-axis and therefore creates an equal superposition state $\frac{1}{\sqrt{2}}(|0\rangle + |1\rangle)$. During the dark phase, the qubit (atom) is described by point C, fixed in the rotating reference frame. The second $\pi/2$ pulse causes the head of the Bloch vector to pass from point C to point B: the two $\pi/2$ pulses give an overall rotation of an angle π. At the end of the two-pulse sequence, the system finds itself in the excited state $|1\rangle$, just as though it had been subject to a single π pulse. Now let's consider the quasi-resonant case, where $\omega \neq \omega_0$, but ω remains sufficiently close to ω_0 that the two pulses are close to being $\pi/2$

pulses. After the first pulse the Bloch vector U is practically in the (u, v) plane and its head is close to point C. Between the first and second pulse, the vector representing the complex field $\tilde{E}$ is fixed along the u-axis, but not the Bloch vector, which turns about w (in the fixed reference frame) at the angular frequency ω_0 and not ω. In the reference frame rotating at frequency ω, at the instant T which marks the beginning of the second pulse, the Bloch vector will have turned by an angle $(\omega_0 - \omega)T$, which is non-negligible if T is sufficiently long. The following cases are particularly important:

1. if $(\omega_0 - \omega)T \equiv \pi \mod (2\pi)$, the qubit will have made a half-turn between the two pulses and will be in a position diametrically opposite its original position, at point D. The second pulse therefore brings the Bloch vector from D to A: the qubit (atom) returns to its original state $|0\rangle$;

2. if $(\omega_0 - \omega)T \equiv 0 \mod (2\pi)$, the qubit will have made a complete turn before the second pulse, and the two rotations will sum again. The atom is transferred to state $|1\rangle$.

A detailed calculation, taking into account the fact that the pulses are not exactly $\pi/2$, shows that the probability of the qubit ending up in the upper state at the end of the two pulses, as a function of the frequency of the applied field, has the form given in figure 3. We observe oscillations, or

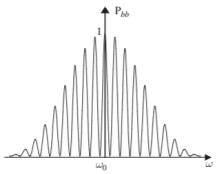

Figure 3: Probability (P) of finding the system excited state after application of two Ramsey pulses of frequency ω.

'fringes', of short period $2\pi/T$, which superpose with the broad resonance (of width $2\pi/t_1$), centred on $\omega = \omega_0$, which we would obtain for a single π pulse of duration t_1. The width of the central peak is therefore linked, not to the qubit–light interaction time, $2t_1$, but to the time between the two pulses

which, respectively, create and read the atomic coherence. For example, if $T = 1$s, the frequency width of the central peak is 1 Hz. This type of response allows us to pinpoint the resonance $\omega = \omega_0$ with a precision better than that obtained with a single pulse. [10]

In summary, the protocol of the Ramsey experiment can be cast as follows (see figure 4 for reference of a possible experiment):

1. The quantum system (qubit) is initialized into $|0\rangle$ state.

2. Using a $\pi/2$ pulse R_1, the qubit is transformed into the superposition state
$$|\psi_0\rangle = |+\rangle \equiv \frac{1}{\sqrt{2}}(|0\rangle + |1\rangle)$$

3. The superposition state evolves for a time t picking up a relative phase $\phi = \omega_0 t$, and the state after the evolution is
$$|\psi(t)\rangle = \frac{1}{\sqrt{2}}(|0\rangle + e^{-i\omega_0 t}|1\rangle)$$
up to an overall phase factor. This operation can be achieved, e.g., by transiently modifying the atomic transition frequency, applying a transient electric or magnetic field. Within an irrelevant global phase factor, this operation produces a phase shift of the atomic coherence, which can be tuned by changing the transient field amplitude or duration.

4. Using a second $\pi/2$ pulse R_2, the state $|\psi(t)\rangle$ is converted back to a measurable state:
$$|\alpha\rangle = \frac{1}{2}(1 + e^{-i\omega_0 t})|0\rangle + \frac{1}{2}(1 - e^{-i\omega_0 t})|1\rangle$$

5. The final state is read out. The transition probability is
$$p = 1 - |\langle 0|\alpha\rangle|^2 = \sin^2(\omega_0 t/2) = \frac{(1 - \cos\omega_0 t)}{2}$$

recording p as a function of time t, an oscillatory output ("Ramsey fringes")

is observed with a frequency given by ω_0. Thus, the Ramsey measurement can directly provide a measurement of the energy splitting (qubit frequency) ω_0. [13]

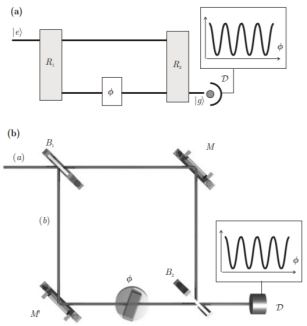

Figure 4: Ramsey Interferometer

The operation of example devices is sketched in figure 4. using a representation mixing time along the horizontal axis with atomic internal state along the vertical axis. [12]

2.3 Fully Quantum-Mechanical Model: The Jaynes–Cummings Model

We now turn to the quantum electrodynamic version of the Rabi model. In our previous pertubation discussion of an atom interacting with a quantized electro-magnetic field, we assumed the field to be a single-mode free field (plane wave). A free atom intereacts with an infinite number of modes and thus the dynamics is not well described assuming only a single-mode field. On the other hand, it has recently become possible to manufacture environments where the density of modes is significantly different than in free space. We have in mind here small microwave cavities, or in some cases, optical cavities capable of supporting only a single mode or maybe a few widely spaced (in frequency) modes. Thus in some cases, the ideal single-mode interaction can be realized in the laboratory. Let's consider a qubit, with levels $|0\rangle$ and $|1\rangle$, interacting with a single-mode cavity field of the form

$$\hat{\mathbf{E}} = \mathbf{e}\Big(\frac{\hbar\omega}{\epsilon_0 V}\Big)^{1/2}(\hat{a} + \hat{a}^\dagger)\sin(kz) \tag{50}$$

where $\mathbf{e}$ is an arbitrarily oriented polarization vector. The interaction Hamiltonian is now

$$\hat{H}^{(I)} = -\hat{\mathbf{d}} \cdot \hat{\mathbf{E}} = \hat{d}g(\hat{a} + \hat{a}^\dagger), \tag{51}$$

where

$$g = -\Big(\frac{\hbar\omega}{\epsilon_0 V}\Big)^{1/2}\sin(kz) \tag{52}$$

is the coupling constant and where $\hat{d} = \hat{\mathbf{d}} \cdot \mathbf{e}$. At this point it is convenient to introduce the so-called atomic transition operators

$$\hat{\sigma}_+ = |1\rangle\langle 0| \tag{53}$$

$$\hat{\sigma}_- = |0\rangle\langle 1| = \hat{\sigma}_+^\dagger \tag{54}$$

and the inversion operator

$$\hat{\sigma}_3 = |1\rangle\langle 1| - |0\rangle\langle 0| \tag{55}$$

There operators obey the Pauli spin algebra

$$[\hat{\sigma}_+, \hat{\sigma}_-] = \hat{\sigma}_3 \tag{56}$$

$$[\hat{\sigma}_3, \hat{\sigma_\pm}] = 2\hat{\sigma}_\pm \tag{57}$$

Only the off diagonal elements of the dipole operator are nonzero, since by parity consideration $\langle 1|\hat{d}|1\rangle = 0 = \langle 0|\hat{d}|0\rangle$, so that we may write

$$\hat{d} = d|0\rangle\langle 1| + d^*|1\rangle\langle 0| = d\hat{\sigma}_- + d^*\hat{\sigma}_+ = d(\hat{\sigma}_+ + \hat{\sigma}_-) \tag{58}$$

where we have the set $\langle 1|\hat{d}|0\rangle = d$ and have assumed, without loss of generality, that d is real. This the interaction Hamiltonian is

$$\hat{H}^{(I)} = \hbar\lambda(\hat{\sigma}_+ + \hat{\sigma}_-)(\hat{a} + \hat{a}^\dagger) \tag{59}$$

where $\lambda = d|0\rangle/\hbar$. If we define the level of the energy to be zero halfway between the states $|0\rangle$ and $|1\rangle$, then the free atomic Hamiltonian may be written as

$$\hat{H}_A = \frac{1}{2}(E_1 - E_0)\hat{\sigma}_3 = \frac{1}{2}\hbar\omega_0\hat{\sigma}_3 \tag{60}$$

where $E_1 = -E_0 = \frac{1}{2}\hbar\omega_0$. The free-field Hamiltonian is, after dropping the zero-point energy term,

$$\hat{H}_F = \hbar\omega\hat{a}^\dagger\hat{a} \tag{61}$$

Thus the total Hamiltonian is

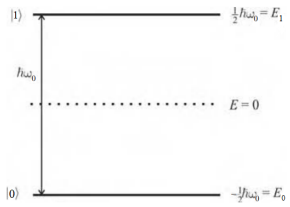

Figure 5: Atomic energy level diagram where the $E = 0$ level is taken halfway between the two levels.

$$\begin{aligned}\hat{H} &= \hat{H}_A + \hat{H}_F + \hat{H}^{(I)} \\ &= \frac{1}{2}\hbar\omega_0\hat{\sigma_3} + \hbar\omega\hat{a}^\dagger\hat{a} + \hbar\lambda(\hat{\sigma}_+ + \hat{\sigma}_-)(\hat{a} + \hat{a}^\dagger)\end{aligned} \tag{62}$$

In the free-field case the operators $\hat{a}$ and $\hat{a}^\dagger$ evolve as

$$\hat{a}(t) = \hat{a}(0)e^{-i\omega t} \tag{63}$$

$$\hat{a}^\dagger(t) = \hat{a}^\dagger(0)e^{i\omega t} \tag{64}$$

One can show similarly for the free-atomic case

$$\hat{\sigma}_\pm(t) = \hat{\sigma}_\pm(0)e^{\pm i\omega_0 t} \tag{65}$$

Thus we can see that the approximate time dependences of the operator products in equation (62) are as follows:

$$\begin{aligned}\hat{\sigma}_+\hat{a} &\sim e^{i(\omega_0-\omega)t} \\ \hat{\sigma}_-\hat{a}^\dagger &\sim e^{-i(\omega_0-\omega)t} \\ \hat{\sigma}_+\hat{a}^\dagger &\sim e^{i(\omega_0+\omega)t} \\ \hat{\sigma}_-\hat{a} &\sim e^{-i(\omega_0+\omega)t}\end{aligned} \tag{66}$$

For $\omega_0 \approx \omega$ the last two terms vary much more rapidly than the first two. Furthermore, the last two terms do not conserve energy in contrast to the first two. The term $\hat{\sigma}_+\hat{a}^\dagger$ corresponds to the emission of a photon as the qubit goes from the ground state to excited state, whereas $\hat{\sigma}_-\hat{a}$ corresponds to the absorbtion of a photon as the atom goes from the excited state to the ground state. Integrating the time-dependent Schrodinger equation, as in the perturbative case, will lead, for the last two terms, to denominators containing $\omega_0 + \omega$ as compared with $\omega_0 - \omega$ for the first two terms. This is the so called rotating wave approximation (RWA). Our Hamiltonian in this approximation is

$$\hat{H} = \frac{1}{2}\hbar\omega_0\hat{\sigma_3} + \hbar\omega\hat{a}^\dagger\hat{a} + \hbar\lambda(\hat{\sigma}_+\hat{a} + \hat{\sigma}_-\hat{a}^\dagger) \tag{67}$$

The interaction described by this Hamiltonian is widely referred to as the Jaynes–Cummings model [11]. Before solving for the dynamics for any specific cases we take note of certain constants of the motion. An obvious one is the number of excitations in the qubit (the electron "number" for the case of atom)

$$\hat{P}_E = |1\rangle\langle 1| + |0\rangle\langle 0| = 1, \tag{68}$$

$$[\hat{H}, \hat{P}_E] = 0 \tag{69}$$

valid when no other atomic states can become populated. Another is the total excitation number (for qubit and the field)

$$\hat{N}_e = \hat{a}^\dagger \hat{a} + |1\rangle\langle 1|, \tag{70}$$

$$[\hat{H}, \hat{N}_e] = 0 \tag{71}$$

Using these constants of the motion we may break the Hamiltonian equation (67) into two commuting parts:

$$\hat{H} = \hat{H}_I + \hat{H}_{II} \tag{72}$$

where

$$\hat{H}_I = \hbar\omega \hat{N}_e + \hbar\Big(\frac{\omega_0}{2} - \omega\Big)\hat{P}_E \tag{73}$$

$$\hat{H}_{II} = -\hbar\Delta + \hbar\lambda(\hat{\sigma}_+ \hat{a} + \hat{\sigma}_- \hat{a}^\dagger) \tag{74}$$

such that $[\hat{H}_I, \hat{H}_{II}] = 0$. Clearly, all the essential dynamics is contained in $\hat{H}_{II}$ whereas $\hat{H}_I$ contributes only overall irrelevant phase factors. Let us now consider a simple example, with $\Delta = 0$, where the atom is initially in the excited state $|1\rangle$ and the field is initially in the number state $|n\rangle$. The initial state of the atom–field system is then $|i\rangle = |1\rangle|n\rangle$ and is of energy $E_i = \frac{1}{2}\hbar\omega + n\hbar\omega$. State $|i\rangle$ is coupled to (and only to) the state $|f\rangle = |0\rangle|n+1\rangle$ with energy $E_f = -\frac{1}{2}\hbar\omega + (n+1)\hbar\omega$. Note that $E_i = E_f$. We write the state

vector as

$$|\psi(t)\rangle = C_i(t)|i\rangle + C_f(t)|f\rangle \tag{75}$$

where $C_i(0) = 1$ and $C_f(0) = 0$. Following standard procedures we obtain, from the interaction picture Schrodinger equation $i\hbar\frac{d|\psi(t)\rangle}{dt} = \hat{H}_{II}|\psi(t)\rangle$ the equations for the coefficients

$$\dot{C}_i = -i\lambda\sqrt{n+1}C_f \tag{76}$$

$$\dot{C}_f = -i\lambda\sqrt{n+1}C_i \tag{77}$$

Eliminating C_f we obtain $\ddot{C}_i + \lambda^2(n+1)C_i = 0$ The solution matching the initial conditions is

$$C_i(t) = \cos(\lambda t\sqrt{n+1}) \tag{78}$$

From equation 76 we obtain

$$C_f(t) = -i\sin(\lambda t\sqrt{n+1}) \tag{79}$$

Thus our solution is

$$|\psi(t)\rangle = \cos(\lambda t\sqrt{N+1})|1\rangle|n\rangle - i\sin(\lambda t\sqrt{n+1})|0\rangle|n+1\rangle \tag{80}$$

The probability that the system remains in the initial state is

$$P_i(t) = |C_i(t)|^2 = \cos^2(\lambda t\sqrt{n+1}) \tag{81}$$

while the probability that it makes a transition to the state $|f\rangle$ is

$$P_f(t) = |C_f(t)|^2 = \sin^2(\lambda t\sqrt{n+1}) \tag{82}$$

The qubit inversion is given by

$$\begin{aligned} W(t) &= \langle\psi(t)|\hat{\sigma}_3|\psi(t)\rangle \\ &= P_i(t) - P_f(t) = \cos(2\lambda t\sqrt{n+1}) \end{aligned} \tag{83}$$

We may define a quantum electrodynamic Rabi frequency $\Omega(n) = 2\lambda\sqrt{n+1}$ so that

$$W(t) = \cos[\Omega(n)t] \tag{84}$$

Clearly, the atomic inversion for the field initially in a number state is strictly periodic (figure 6), just like in the semicalssical case and except for thr fact that in the classical case there must always be a field present initially. But

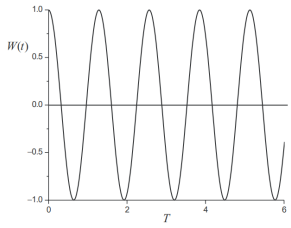

Figure 6: Periodic atomic inversion with the field initially in a number state $|n\rangle$ with n = 5 photons

in the quantum-mechanical case there are Rabi oscillations even for the case when $n = 0$. These are the vacuum-field Rabi oscillations and, of course, they have no classical counterpart. They are the result of the atom spontaneously emitting a photon then re-absorbing it, re-emitting it, etc.: an example of reversible spontaneous emission. Such effects can be observed if atoms interact with fields in very high Q cavities. But aside from this, overall, the behavior of the atomic dynamics for a definite number of photons is very much like the semiclassical Rabi model, i.e. it is periodic and regular. Perhaps this is a bit counterintuitive since a number state is the most nonclassical of all the field states. Intuition might suggest that when the field is initially in a coherent state, we should recover the semiclassical, periodic and regular, Rabi oscillations. As we are about to demonstrate, intuition, in this case, fails. Let us now consider a more general (pure state) solution of the dynamics. We assume the atom is initially in a superposition of states $|1\rangle$ and $|0\rangle$:

$$|\psi(0)\rangle_{\text{qubit}} = C_0|0\rangle + C_1|1\rangle \tag{85}$$

and the field is initially in the state

$$|\psi(0)\rangle_{\text{field}} = \sum_{n=0}^{\infty} C_n |n\rangle \tag{86}$$

such that the initial qubit-field state is

$$|\psi(0)\rangle = |\psi(0)\rangle_{\text{qubit}} \otimes |\psi(0)\rangle_{\text{field}} \tag{87}$$

The solution of the Schrodinger equation is now

$$\begin{aligned} |\psi(t)\rangle = \sum_{n=0}^{\infty} \Big\{ \Big[C_1 C_n \cos(\lambda t\sqrt{n+1}) - iC_0 C_{n+1} \sin(\lambda t\sqrt{n+1}) \Big] |1\rangle \\ + \Big[-iC_1 C_{n-1} \sin(\lambda t\sqrt{n}) + C_0 C_n \cos(\lambda t\sqrt{n}) \Big] |0\rangle \Big\} |n\rangle \end{aligned} \tag{88}$$

In general, this is an entangled state. For the case of the qubit initially in the excited state, where $C_1 = 1$ and $C_0 = 0$, we may write the solution as

$$|\psi(t)\rangle = |\psi_1(t)\rangle|1\rangle + |\psi_0(t)\rangle|0\rangle \tag{89}$$

where $|\psi_1(t)\rangle$ and $|\psi_0(t)\rangle$ are the field components of $|\psi(t)\rangle$ given by

$$|\psi_0(t)\rangle = -i \sum_{n=0}^{\infty} C_n \sin(\lambda t\sqrt{n+1}) |n+1\rangle, \tag{90}$$

$$|\psi_1(t)\rangle = \sum_{n=0}^{\infty} C_n \cos(\lambda t\sqrt{n+1}) |n\rangle \tag{91}$$

The qubit inversion is

$$\begin{aligned} W(t) &= \langle\psi(t)|\hat{\sigma}_3|\psi(t)\rangle \\ &= \langle\psi_1(t)|\psi_1(t)\rangle - \langle\psi_0(t)|\psi_0(t)\rangle \\ &= \sum_{n=0}^{\infty} |C_n|^2 \cos(2\lambda t\sqrt{n+1}) \end{aligned} \tag{92}$$

The result is just the sum of n-photon inversions of equation (83) weighted

with the photon number distribution of the initial field state. For the coherent state, again that most classical of all quantum states, we have

$$C_n = e^{-|\alpha|^2/2}\frac{\alpha^n}{\sqrt{n!}} \tag{93}$$

and the inversion is

$$W(t) = e^{-\bar{n}}\sum_{n=0}^{\infty}\frac{\bar{n}^n}{n!}\cos(2\lambda t\sqrt{n+1}) \tag{94}$$

A plot of W(t) versus the scaled time $T = \lambda t$ in figure. 7 reveals significant discrepancies between the fully quantized and semiclassical Rabi oscillations. We note first that the Rabi oscillations initially appear to damp out, or collapse. The collapse of the Rabi oscillations was noted fairly early in the study of this "idealized" model interaction. Several years later, perhaps by executing longer runs of a computer program, it was found that after a period of quiescence following the collapse, the Rabi oscillations start to revive, although not completely. At longer times one finds a sequence of collapses and revivals, the revivals becoming less distinct as time increases. This collapse and revival behavior of the Rabi oscillations in the fully quantized model is strikingly different than in the semiclassical case where the oscillations have constant amplitude. We must now explain this difference. First we consider

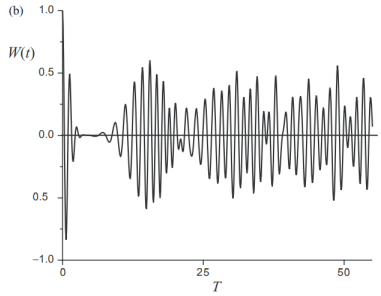

Figure 7: Atomic inversion with the field initially in a coherent state $\bar{n} = 5$. Here, T is the scaled time λt.

the collapse. The average photon number is $\bar{n} = |\alpha|^2$ so the dominant Rabi

frequency is

$$\Omega(\bar{n}) = 2\lambda\sqrt{\bar{n}+1} \approx 2\lambda\sqrt{\bar{n}}, \quad \bar{n} \gg 1 \tag{95}$$

But there will be a range of "important" frequencies as a result of the spread of the probabilities $|C_n|^2$ about $\bar{n}$ for photon numbers in range $\bar{n} \pm \Delta n$; i.e. the frequencies in the range $\Omega(\bar{n} - \Delta n)$ to $\Omega(\bar{n} + \Delta n)$. The collapse time t_c may be estimated from the time-frequency "uncertainty" relation

$$t_c[\Omega(\bar{n} + \Delta n) - \Omega(\bar{n} - \Delta n)] \simeq 1 \tag{96}$$

where the spread of frequencies is responsible for the "dephasing" of the Rabi oscillations. For the coherent state, $\Delta n = \bar{n}^{1/2}$, and with

$$\begin{aligned} \Omega(\bar{n} \pm n^{-1/2}) &\simeq 2\lambda[\bar{n} \pm \bar{n}^{1/2}]^{1/2} = 2\lambda\bar{n}^{1/2}\Big[1 \pm \frac{1}{\bar{n}^{1/2}}\Big] \\ &\simeq 2\lambda\bar{n}^{1/2}\Big[1 \pm \frac{1}{2\bar{n}^{1/2}}\Big] = 2\lambda\bar{n}^{1/2} \pm \lambda, \end{aligned} \tag{97}$$

it follows that

$$t_c[\Omega(\bar{n} + \bar{n}^{1/2}) - \Omega(\bar{n} - \bar{n}^{1/2})] \simeq t_c 2\lambda \simeq 1, \tag{98}$$

and thus $t_c \simeq (2\lambda)^{-1}$, which is independent of $\bar{n}$. The preceding "derivation" of the collapse time is not very rigorous. A more rigorous derivation yields $t_c = \frac{\sqrt{2}}{\lambda}\sqrt{\frac{\bar{n}+1}{\bar{n}}} \simeq \frac{\sqrt{2}}{\lambda}, \quad (\bar{n} \gg 1)$.

2.4 Dynamical Decoupling

Quantum information processing requires overcoming decoherence – the loss of "quantumness" due to the inevitable interaction between the quantum system and its environment. One approach towards a solution is quantum dynamical decoupling – a method employing strong and frequent pulses applied to the qubits [14]. Dynamical decoupling pulse sequences have been used to extend coherence times in quantum systems ever since the discovery of the spin-echo effect. There are two possible pulse sequences for dynamical decoupling method. First one is the concatenated dynamical decoupling (CDD) and the periodic dynamical decoupling (PDD). It can be shown that CDD is significantly more efficient at decoupling than PDD, when compared at equal switching times and pulse numbers [15].

Noise can be categorized into two primary types – systematic noise and stochastic noise. We will focus on error mitigation strategies that address stochastic noise. Stochastic noise is the random fluctuation of a parameter that is coupled to the qubit, and it can cause decoherence in different ways. A qubit in state $|1\rangle$ can relax to the ground state by losing energy to its environment with a rate $\Gamma_1 = 1/T_1$, where T_1 is the relaxation time. There is also decoherence of the Bloch vector on the equator, as characterized by the decoherence rate $\Gamma_2 = 1/T_2$. On the equator, there are two things that can go wrong. First, the qubit could simply relax back to the ground state via a T_1 process. And clearly, this is a phase-breaking event, since once the Bloch vector has relaxed to the north pole ($|0\rangle$ state), there's no way to tell which direction it had been pointing when it was on the equator. And second, the Bloch vector can diffuse around the equator which is called dephasing. The decoherence time, T_2, is a combination of both the dephasing time, T_φ, and the relaxation time, T_1. Note that if there is no dephasing, such that T_φ becomes very large, then $T_2 = 2T_1$ and is completely limited by relaxation. While energy relaxation processes are generally irreversible, dephasing processes may in fact be coherent, and therefore reversible. Coherent dephasing errors can be mitigated using dynamical decoupling pulse sequences, a type of passive error suppression (see figure 8).

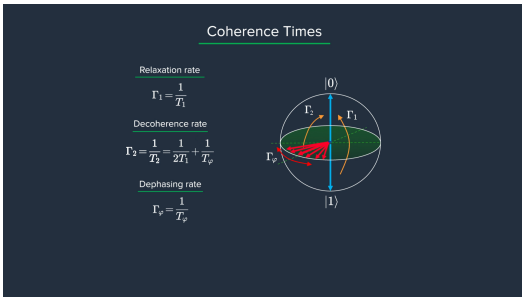

Figure 8: Coherence Times

We will take as an example a superconducting flux qubit. The flux qubit shown in figure9 is a superconducting loop interrupted by 4 Josephson junctions. Threading a magnetic flux through the loop sets the qubit energy level E_{01}. However, due to local magnetic field fluctuations in the qubit's environment, the energy levels also fluctuate, and this leads to qubit dephasing. To

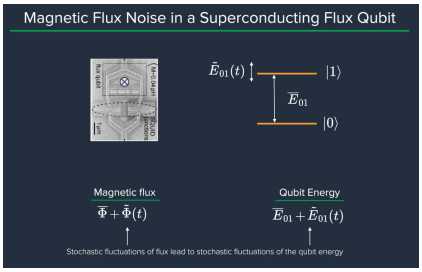

Figure 9: Magnetic Flux Noise in a Superconducting Qubit

see this, let's take a qubit to be in a superposition state

$$\alpha|0\rangle + \beta|1\rangle \tag{99}$$

Because state $|1\rangle$ is at a higher energy than state $|0\rangle$, it acquires phase at a faster rate. So we can rewrite 99 as

$$\alpha|0\rangle + \beta|1\rangle \rightarrow \alpha|0\rangle + \beta e^{i\varphi(t)}|1\rangle \tag{100}$$

where

$$\varphi(t) = \frac{E_{01}}{\hbar}t \tag{101}$$

This is called free evolution because the phase of the qubit evolves solely due to the energy level difference and not due to any external driving. Now, in the absence of noise, E_{01} is fixed, and so the phase acquire is deterministic, meaning that at any time t in the future, we can tell precisely the value of the phase. However, in the presence of noise, such as low frequency flux noise due to the local magnetic environment of the qubit, the energy level separation will fluctuate. There's now an average value of the energy, $\bar{E}_{01}$, corresponding to an average phase, $\bar{\varphi}$. But due to the stochastic noise, there is also a fluctuating energy, $\tilde{E}_{01}$, which fluctuates in time (see figure 10). And

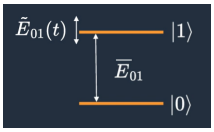

Figure 10: The Energy Levels of the Qubit

this corresponds to a fluctuating phase, $\tilde{\varphi}(t)$. So the value of $\varphi(t)$ will be

$$\varphi(t) = \bar{\varphi}(t) + \tilde{\varphi}(t), \;\; \bar{\varphi}(t) = \frac{\bar{E}_{01}}{\hbar} t. \tag{102}$$

It is this stochastic phase which leads to dephasing. We can write an expression for the resulting dephasing in an intuitive form by looking at the ensemble average of the dephasing.

$$\begin{aligned} \left\langle e^{i\tilde{\varphi}(t)} \right\rangle &= \left\langle e^{\frac{i}{\hbar}} \int_0^t d\tau \tilde{E}_{01}(\tau) \right\rangle \\ &= \exp\Big[-\frac{t^2}{2\hbar^2} \Big(\frac{\partial E_{01}}{\partial \Phi} \Big)^2 \int d\omega S_\Phi(\omega) g_N(\omega t) \Big]. \end{aligned} \tag{103}$$

Phase accrues in an exponent, as $e^{i\varphi}$, and the phase at time t is the time integral of the energy fluctuation, $\tilde{E}_{01}$. In taking the ensemble average, we'll assume that the noise is Gaussian-distributed, that is, arising from a large number of weakly coupled magnetic noise sources, and this leads to the following intuitive result 103. First off, we have the change in energy due to the fluctuations, which we will assume here are fluctuations in the magnetic flux, Φ. This is the sensitivity of the qubit energy to fluctuations in magnetic

flux, squared. Next is the strength of the magnetic flux noise that drives the energy fluctuations. This is the integral over frequency of the noise power spectral density, and it has units of Φ^2. By itself, this would simply be the variance of the noise process. The noise power spectral density $g_N(\omega t)$ is shaped by a term called the filter function. The filter function depends on the pulse sequence that we apply to the qubit, and it serves to filter, or window, the noise.

3 Experimental Part: Calibrating Qubits and Pulses

In this section I will apply what we have learned theoretically in the previous parts. I will use IBM Quantum computer to make the experiments for finding and measuring the qubit frequency, calibrate π pulse, measure relaxation time T_1 and dephasing time T_2, and, finally, apply dynamical decoupling technique for noise elimination. The code implementation can be found in my github account [16].

3.1 Finding Qubit Frequency Using Frequency Sweep

We begin by searching for the qubit frequency. The qubit frequency is the difference in energy between the ground and excited states, which we label the $|0\rangle$ and $|1\rangle$ states, respectively. This frequency will be crucial for creating pulses which enact particular quantum operators on the qubit – the final goal of our calibration. With superconducting qubits, higher energy levels are also available, but the systems are fabricated to be anharmonic so that one can control which transition one is exciting. That way, one is able to isolate two energy levels and treat each qubit as a basic two-level system, ignoring higher energy states.

In a typical lab setting, the qubit frequency can be found by sweeping a range of frequencies and looking for signs of absorption using a tool known as a Network Analyzer. This measurement gives a rough estimate of the qubit frequency. Later on, we will see how to do a more precise measurement using a Ramsey pulse sequence.

One can define the pulses for experiment. We will start with the drive pulse, which is a Gaussian pulse of width 0.075μ truncated at 4 standard deviations from both sides of the mean.

Now we can define our measurement pulse Now that the pulse parameters have been defined, and we have created the pulse shapes for our experiments, we can proceed to create the pulse schedules.

At each frequency, we will send a drive pulse of that frequency to the qubit and measure immediately after the pulse.

As a sanity check, it's always a good idea to look at the pulse schedule (See figure 11). We assemble the schedules that can be sent to the quantum

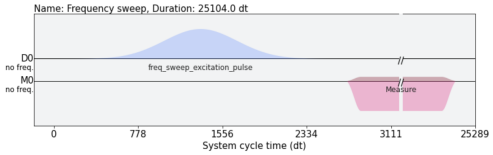

Figure 11: Result of the program

device. We request that each schedule (each point in our frequency sweep) is repeated predefined number of times (e.g., 1024) in order to get a good estimate of the qubit response.

Once the job is run, the results can be retrieved. As you can see, the dip near the center corresponds to the location of the qubit frequency. The signal shows power-broadening, which is a signature that we are able to drive the qubit off-resonance as we get close to the center frequency. To get the value of the peak frequency, we will fit the values to a resonance response curve, which is typically a Lorentzian shape. You can also see the fitted plot from which we retrieve/update qubit frequency from previous 4.9717 to 4.97181 GHz.

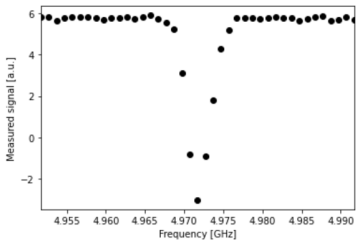

(a) Result of the program

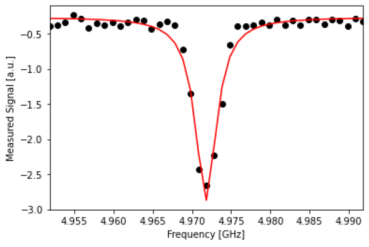

(b) Fitted result of the program

3.2 Calibrating π Pulses Using a Rabi Experiment

Once we know the frequency of our qubit, the next step is to determine the strength of a π pulse. Strictly speaking of the qubit as a two-level system, a π pulse is one that takes the qubit from $|0\rangle$ to $|1\rangle$, and vice versa. This is also called the X gate or bit-flip operator. We already know the microwave frequency needed to drive this transition from the previous frequency sweep experiment, and we now seek the amplitude needed to achieve a π rotation from $|0\rangle$ to $|0\rangle$. The desired rotation is shown on the Bloch sphere in the figure 14 – you can see that the π pulse gets its name from the angle it sweeps over on a Bloch sphere. We will change the drive amplitude in small increments

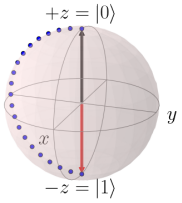

Figure 13: π Rotation on the Bloch Sphere

and measuring the state of the qubit each time. We expect to see oscillations which are commonly named Rabi oscillations, as the qubit goes from $|0\rangle$ to $|1\rangle$ and back. This experiment uses these values from the previous experiment, additionally, drive amplitude values are iterated over 50 amplitudes evenly spaced from 0 to 0.75. When building the Rabi experiments, a drive pulse is set at the qubit frequency, followed by a measurement, where we vary the drive amplitude each time.

The schedule will look essentially the same as the frequency sweep experiment, see figure 14. The only difference is that we are running a set of experiments which vary the amplitude of the drive pulse, rather than its modulation frequency.

Now that we have our results, we will extract them and fit them to a sinusoidal curve. For the range of drive amplitudes we selected, we expect that we will rotate the qubit several times completely around the Bloch sphere, starting from $|0\rangle$. The amplitude of this sinusoid will tell us the

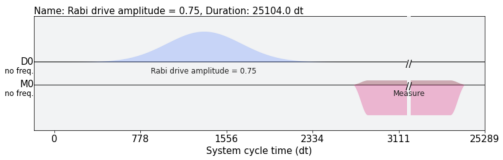

Figure 14: Rabi's experiment schedule

fraction of the shots at that Rabi drive amplitude which yielded the $|1\rangle$ state. We want to find the drive amplitude needed for the signal to oscillate from a maximum (all $|0\rangle$ state) to a minimum (all $|1\rangle$ state) – this gives the calibrated amplitude that enacts a π pulse. From the fitted curve, we derive that the pulse amplitude is 0.140753.

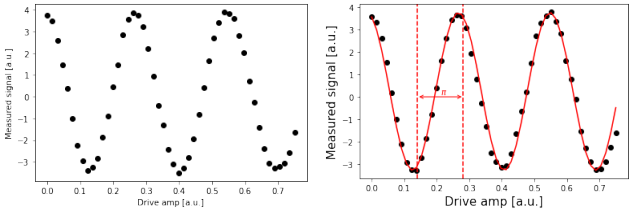

(a) Rabi's experiment schedule

(b) Fitting the cosine curve

3.3 Determining 0 vs 1

Once our π pulses have been calibrated, we can now create the state $|1\rangle$ with good probability. We can use this to find out what the states $|0\rangle$ and $|1\rangle$ look like in our measurements, by repeatedly preparing them and plotting the measured signal. The figure below shows the two cases: initialize to $|0\rangle$ and measure, and initialize to $|0\rangle$ and apply a π pulse to get $|1\rangle$ state, then measure. This experiment is repeated 1024 times.

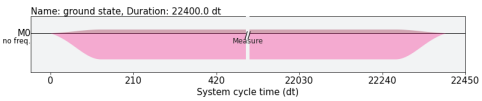

(a) Pi pulse amplitude

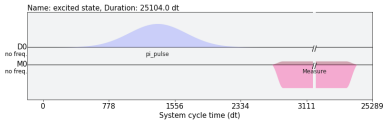

(b) Pi pulse amplitude

Now that we have the results, we can visualize the two populations which we have prepared on a simple scatter plot, showing results from the ground state program in blue and results from the excited state preparation program in red, see figure 18. We can clearly see that the two populations of $|0\rangle$ and

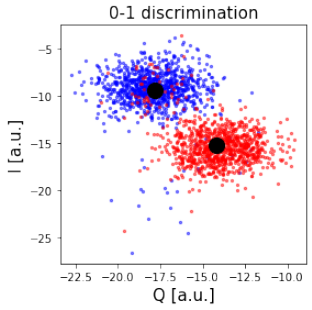

Figure 17: 0-1 Discrimination

$|1\rangle$ form their own clusters.

3.4 Measuring T_1 Using Inversion Recovery

The T_1 time of a qubit is the time it takes for a qubit to decay from the excited state to the ground state. It is important because it limits the duration of meaningful programs we can run on the quantum computer.

Measuring T_1 is similar to our previous experiments, and uses the π pulse we've calibrated. We again apply a single drive pulse, our π pulse, then apply a measure pulse. However, this time we do not apply the measurement immediately. We insert a delay of $6\mu s$, and vary that delay between experiments up to 450 μs. When we plot the measured signal against delay time, we will see a signal that decays exponentially as the qubit relaxes in energy. The decay time is the T_1, or relaxation time, of the qubit.

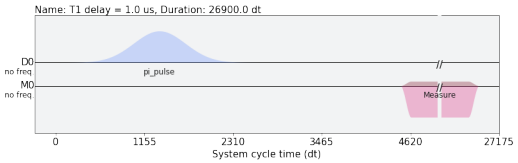

Figure 18: T_1 experiment schedule

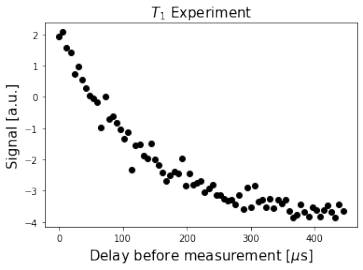

(a) Plot

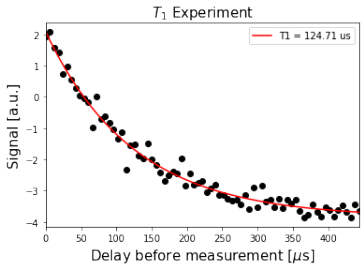

(b) Fitted plot

We can then fit the data to a decaying exponential, giving us T_1.

3.5 Measuring the Qubit Frequency Precisely Using a Ramsey Experiment

Now, we determine the qubit frequency to better precision. This is done using a Ramsey pulse sequence. In this pulse sequence, we first apply a $\pi/2$ ("pi over two") pulse, wait some time Δt, and then apply another $\pi/2$ pulse. Since we are measuring the signal from the qubit at the same frequency as the pulses, we should observe oscillations at the difference in frequency between the applied pulses and the qubit.

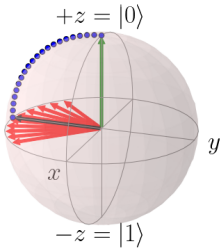

Figure 20: Ramsay Experiment Bloch Sphere

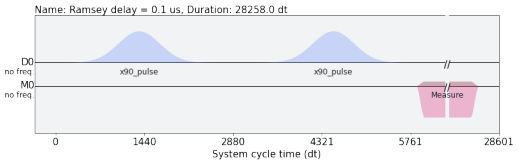

Figure 21: Ramsay Experiment Schedule

Here, we will apply a commonly used experimental trick. We will drive the pulses off-resonance by a known amount, which we will call detuning in MHz. The measured Ramsey signal should show oscillations with frequency near detuning in MHz, with a small offset. This small offset is exactly how far away rough qubit frequency was from the qubit frequency.

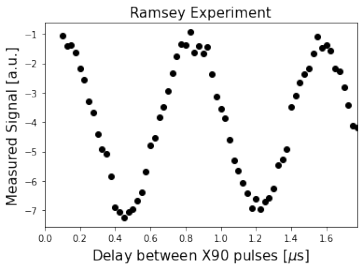

(a) Ramsay Experiment Plot

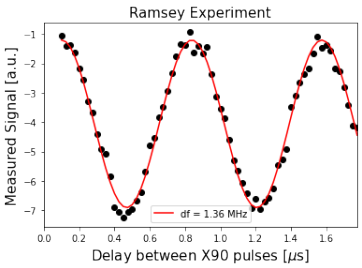

(b) Ramsay Experiment Fit

Now that we know df in MHz, we can update our estimate of the qubit frequency.

3.6 Measuring T_2 Using Hahn Echoes

Next, we can measure the coherence time, T_2, of our qubit. The pulse sequence used to do this experiment is known as a Hahn echo, a term that comes from the NMR community. A Hahn echo experiment is very similar to the Ramsey experiment above, with an additional π pulse between the two $\pi/2$ pulses. The π pulse at time τ reverses the accumulation of phase, and results in an echo at time 2τ, where we apply the last $\pi/2$ pulse to do our measurement.

The decay time for the Hahn echo experiment gives us the coherence time, T_2.

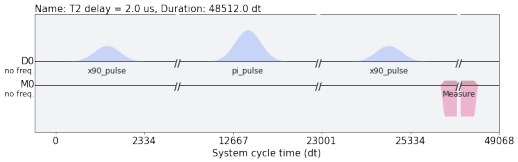

Figure 23: Hahn Echo Experiment Schedule

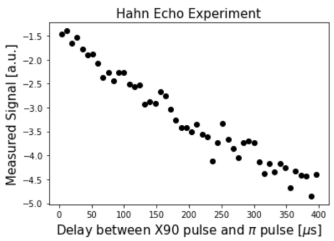

(a) Hahn Echo Experiment Plot

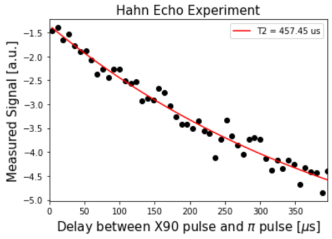

(b) Hahn Echo Experiment Fit

3.7 Dynamical Decoupling

A single π pulse is able to eliminate quasi-static noise due to the reversal of phase accumulation. This concept can be extended to noise that cannot be approximated as quasi-static by applying several π pulses in succession. This technique, commonly known as dynamical decoupling (DD), allows us to cancel different frequencies of noise and is used to extract longer coherence times from qubits. In standard DD, one uses a periodic sequence of fast and strong symmetrizing pulses to reduce the undesired interaction of the system and its environment causing decoherence. The first figure below shows an example shot of 6 π pulses between 2 $\pi/2$ pulses in a Ramsey experiment. The second figure represents the signal strength over the total time when the time between pulses is increased in every consecutive experiment similar the one in the above picture. The fitted curve then gives an estimate of T_2 which is longer than that of without DD technique applied.

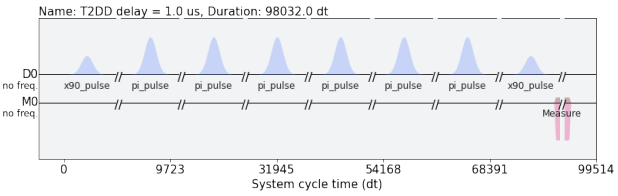

Figure 25: Schedule of Dynamical Decoupling

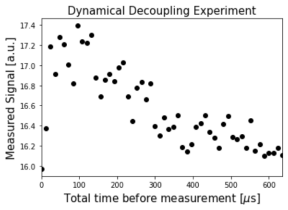

(a) Dynamical Decoupling Experiment

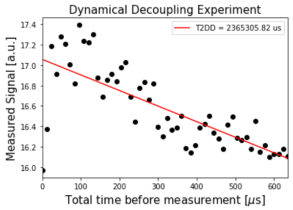

(b) Fitting the Dynamical Decoupling

4 Conclusion

After looking through the theory for the two-level systems and proving that qubits can definitely be described with that theories, we have stated the Rabi's and Ramsey's experiments and mitigated the errors using dynamical decoupling. Afterwards we have done experiments on the quantum computer of IBM, including finding the qubit frequency using frequency sweep algorithm, afterwards finding the best amplitude by doing the Rabi π-pulse experiment. After finding our perfect π-pulse we have measured the T_1 and T_2, done the Ramsey experiment and eventually decreased the errors using dynamical decoupling. By comparing the theory with the experiment, it can be seen that the theory for the two-level systems perfectly works for the qubits. Overall after calibrating the pulse for 1 qubit there are plenty of other opportunities including implementing gates for multiple qubits.

References

[1] D. P. DiVincenzo, "Quantum Computation", Science **270**, 255 (1995).

[2] E. Knill et. al., "Introduction to Quantum Information Processing", arXiv:quant-ph/0207171 (2002).

[3] https://quantumalgorithmzoo.org/

[4] https://www.dwavesys.com/

[5] S. Lloyd "Universal quantum simulators", Science **273**, 1073 (1996).

[6] T. D. Ladd et. al., "Quantum computers" nature **464**, 45 (2010).

[7] IBM Quantum. https://quantum-computing.ibm.com/composer/docs/iqx/guide/the-qubit

[8] Cohen-Tannoudji C., Diu B., Laloe F., "Quantum mechanics", page 405 (1992)

[9] N. Ramsey, "A Molecular Beam Resonance Method with Separated Oscillating Fields". Phys. Rev. **78**, 695 (1950).

[10] Gilbert Grynberg, Alain Aspect, Claude Fabre "Introduction to Quantum Optics", Cambridge University Press, page 168, (2010).

[11] Christopher Gerry, Peter Knight "Introductory Quantum Optics", Cambridge University Press, page 90 (2005).

[12] Serge Haroche, Jean-Michel Raimond, "Exploring the Quantum", Oxford University Press, page 149 (2006).

[13] C. L. Degen, F. Reinhard, and P. Cappellaro, "Quantum sensing". Rev. Mod. Phys. **89**, 035002, (2017).

[14] X. Peng, D. Suter, D. Lidar, "High Fidelity Quantum Gates via Dynamical Decoupling". Phys. Rev. Lett. **105**, 230503 (2011).

[15] K. Khodjasteh, D.A. Lidar, "Fault-Tolerant Quantum Dynamical Decoupling", Phys. Rev. Lett. **95**, 180501 (2005).

[16] The github code for the experiments.
https://github.com/UndineStein/qiskit_pulse_experiment/tree/master